Journal of
Materials Chemistry C

PAPER

View Article Online
View Journal | View Issue

Cite this: *J. Mater. Chem. C*, 2016, 4, 6391

Bis(2-oxoindolin-3-ylidene)-benzodifuran-dione and bithiophene-based conjugated polymers for high performance ambipolar organic thin-film transistors: the impact of substitution positions on bithiophene units†

Xiaohong Wang,[ab] Hyun Ho Choi,[c] Guobing Zhang,*[ab] Yunsheng Ding,*[b] Hongbo Lu,[ab] Kilwon Cho[c] and Longzhen Qiu*[ab]

Received 21st April 2016, Accepted 6th June 2016

DOI: 10.1039/c6tc01617k

www.rsc.org/MaterialsC

Three donor–acceptor polymers based on (3*E*,7*E*)-3,7-bis(2-oxoindolin-3-ylidene)benzo-[1,2-*b*:4,5-*b*]-difuran-2,6(3*H*,7*H*)-dione (**BIBDF**) and three kinds of dialkylated bithiophenes with head-to-head (HH), head-to-tail (HT), and tail-to-tail (TT) connectivity were synthesized by the Stille coupling reaction. Their photophysical and electrochemical properties, electronic device performance, and microstructure were investigated. We found that the alkyl chains substituted near the thiophene–thiophene connection cause less steric hindrance than those near the **BIBDF**–thiophene connection. Therefore **PBIBDF-HH** exhibited the preferred planarity, crystallinity, and molecular orientation, yielding the highest field-effect mobility. A maximum electron mobility of 1.23 cm^2 V^{-1} s^{-1} and a maximum hole mobility of 0.37 cm^2 V^{-1} s^{-1} were obtained for **PBIBDF-HH**-based devices. These results show that the substitution sites on the bithiophene units play an important role in the determination of molecular organization and the resulting device performance.

1. Introduction

A need for low-cost, large-area, and flexible electronics such as displays and sensor tags has generated considerable interest in organic thin-film transistors (OTFTs) over the last decade.[1–3] Solution-processed conjugated polymers are particularly suitable for these applications because they can be fabricated on flexible substrates over a large area at low cost using roll-to-roll or ink-jet printing techniques.[4–6] However the carrier mobilities of polymers were typically lower than those of inorganic semiconductors and insoluble organic small molecules such as pentacene. The recent combined efforts in materials design and device processing/fabrication optimization have improved the performance of OTFTs based on solution-processed conjugated polymers with charge carrier mobilities reaching as high as 23.7 cm^2 V^{-1} s^{-1} in the past few years.[7–11] Several π-conjugated building blocks with rigid and coplanar structures have been developed to design and synthesize high performance polymer semiconductors, including electron-rich aromatic units, such as thio(seleno)phene,[12] fused thio(seleno)phene,[13]and vinylene,[10,14] and electron-deficient units such as benzothiadiazole,[7,15] naphthalene diimide,[1,16–21] benzobisthiadiazole,[22,23] diketopyrrolopyrrole,[9,12,24–34] and isoindigo.[8,35–38] Generally, the use of these rigid building blocks in conjugated polymers can induce strong intermolecular interactions and dense long-range orientation of the polymer backbone, resulting in superior charge carrier mobility. The rigid fused building blocks however can reduce the solubility and solution processability of the polymeric semiconductors. The general strategy to address this problem is to incorporate alkyl side chains into the conjugated backbones to tune their solubility. As insulating moieties, these flexible side chains that primarily function as solubilizing groups do not generally contribute directly to charge transport in the conjugated polymers. Recently, more and more studies have exploited the substantial impact of the flexible side chains in organic semiconductors.[13,30,39–43] The results showed that even subtle changes in the flexible side

---

[a] *Key Lab of Special Display Technology, Ministry of Education, National Engineering Lab of Special Display Technology, State Key Lab of Advanced Display Technology, Academy of Opto-Electronic Technology, Hefei University of Technology, Hefei, 230009, China. E-mail: gbzhang@hfut.edu.cn, lzhqiu@hfut.edu.cn*

[b] *Anhui Key Laboratory of Advanced Functional Materials and Devices, School of Chemistry and Chemical Engineering, Hefei University of Technology, Hefei, 230009, China. E-mail: dingys@hfut.edu.cn*

[c] *Department of Chemical Engineering, Pohang University of Science and Technology, Pohang, 790-784, Korea. E-mail: kwcho@postech.ac.kr*

† Electronic supplementary information (ESI) available. See DOI: 10.1039/c6tc01617k

chains can significantly alter the intermolecular interactions, thin-film packing and charge carrier transport. Although numerous side chain substituents have been developed to date, their potential functions have not been fully investigated because of their complexity and strong dependence on the conjugated backbone.

(3*E*,7*E*)-3,7-Bis(2-oxoindolin-3-ylidene)benzo-[1,2-*b*:4,5-*b*′]-difuran-2,6(3*H*,7*H*)-dione (**BIBDF**), also named as benzodifurandione-based oligo(*p*-phenylenevinylene) (BDOPV), is a derivative of isoindigo.[44,45] The electron-deficient lactone groups and lactam groups in the **BIBDF** unit significantly decrease the LUMO level to a value of −4.24 eV. As a result, conjugated polymers based on **BIBDF** always exhibit low LUMO and HOMO energy levels, making them suitable for ambipolar or n-type OTFTs. Bithiophene is a well-known building block for high-performance conjugated polymers in polymer solar cells and OTFTs. Donor–acceptor (D–A) polymers based on bithiophene (BT) and **BIBDF** units were first reported by Li *et al.*[46] The **BIBDF**–BT polymer however exhibited such strong intermolecular interactions and was essentially insoluble in any solvent. Pei *et al.*[47] reported the first soluble **BIBDF**–BT polymer by increasing the length of the **BIBDF** branched chains. They reported n-type transport under ambient conditions with electron mobilities up to 1.74 $cm^2 V^{-1} s^{-1}$ and ambipolar charge transport under oxygen exposure with the electron and hole mobilities of up to 1.45 and 0.47 $cm^2 V^{-1} s^{-1}$, respectively. However, a great challenge is faced in synthesizing and purifying such long, branched alkyl chains.

Recently, we demonstrated that introducing solubilizing alkyl chains into the bithiophene unit provides an alternative method to obtain a soluble **BIBDF**–BT polymer.[48] Previous studies revealed that, for the isoindigo-(IID) and diketopyrrolopyrrole-(DPP) based polymers, the alkyl chain substituted on the bithiophene units can cause steric hindrance and hinder the π–π stacking of the chain segment, severely reducing the charge carrier mobility.[49] However, our **BIBDF**–BT polymer with alkyl chains on the bithiophene unit showed hole mobilities of up to 0.30 $cm^2 V^{-1} s^{-1}$, and electron mobilities of up to 1.08 $cm^2 V^{-1} s^{-1}$, comparable to those reported by Pei *et al.*[47] These observations indicate that the impact of flexible side chains on conjugated polymers may correlate with their backbone building blocks.

In this investigation, we designed and synthesized three **BIBDF**–BT polymers substituted with dodecyl side chains in different positions and investigated the effect of the side chain position on the microstructure and field-effect properties. The influence of the position on molecular packing, crystallization and field-effect properties of the corresponding transistors was also investigated.

2. Experimental section

2.1. Materials

The materials used in this experiment were purchased form Sigma-Aldrich Chemical Company and Alfa Aesar Chemical Company. Toluene and tetrahydrofuran were freshly distilled prior to use.

2.2. Fabrication and characterization of field-effect transistors

Top-contact bottom-gate OTFT devices were fabricated on 300 nm SiO_2. SiO_2 was thermally grown on highly n-doped silicon. A 20 nm CYTOP polymer layer was spin-coated on SiO_2. A 5 mg ml^{-1} chloroform solution of the semiconductor polymer was spin-coated at 3500 rpm. The thickness of the obtained film as measured by atomic force microscopy (AFM) is about 80 nm. The polymer films were subsequently annealed at 100, 150, 175, and 200 °C for 30 minutes under a nitrogen atmosphere. Au source–drain electrodes (approximately 50 nm thick) were then evaporated on the semiconductor layers.

The channel length of the OTFT is 100 μm and the channel width is 1 mm. The electrical testing of the OTFT devices was performed under vacuum using a Keithley 4200 Parameter Analyzer. The electron (μ_e) and hole (μ_h) mobilities were obtained according to the following equation in the saturation regime: $I_d = (W/2L)C_i\mu_{h \text{ or } e}(V_g - V_{th})^2$, where I_d is the drain current in the saturated regime, W is the channel length, L is the channel width, C_i is the capacitance of the dielectrics, and V_{th} is the threshold voltage. At least 12 transistors are fabricated to characterize the field-effect performance of the polymers.

2.2. Instrumentation

Nuclear magnetic resonance (NMR) spectra were obtained from a VNMRS600 MHz machine. Gel permeation chromatography (GPC) was performed on a Waters Series 1525 gel chromatography system coupled with a UV-vis detector using 1,2,4-trichlorobenzene as an eluent at 100 °C. UV-vis absorption spectra were performed on a Perkin Elmer model λ 20 UV-vis spectrophotometer. Electrochemical measurements were conducted on a CHI 660D electrochemical analyzer under nitrogen in deoxygenated anhydrous acetonitrile solution of tetra-*n*-butylammoniumhexafluorophosphate (0.1 M). A platinum wire was used as an auxiliary electrode, a platinum-disc electrode was used as a working electrode, and an Ag/Ag^+ electrode was used as a reference electrode. Polymer thin films were coated onto the platinum-disc electrode and ferrocene was used as a reference. The grazing-incidence X-ray diffraction (GIXD) studies were performed using 3C beamlines at the Pohang Accelerator Laboratory (PLA) in Korea and BL16B beamlines at the Shanghai Synchrotron Radiation Facility (SSRF) in China. Tapping AFM was performed using a Veeco multimode instrument.

3. Results and discussion

3.1. Synthesis and characterization

Scheme 1 presents the synthesis route of the three polymers. The dibromo-monomer **BIBDF**,[48] head-to-head coupled 5,5′-bis(trimethylstannyl)-3,3′-bis(dodecyl)-2,2′-bithiophene (**M$_1$**), head-to-tail coupled 5,5′-bis(trimethylstannyl)-3,4′-bis(dodecyl)-2,2′-bithiophene (**M$_2$**), and tail-to-tail coupled 5,5′-bis(trimethylstannyl)-4,4′-bis(dodecyl)-2,2′-bithiophene (**M$_3$**) were synthesized according to previous literature.[48,50,51] Three polymers with head-to-head (**PBIBDF-HH**), head-to-tail (**PBIBDF-HT**), and tail-to-tail

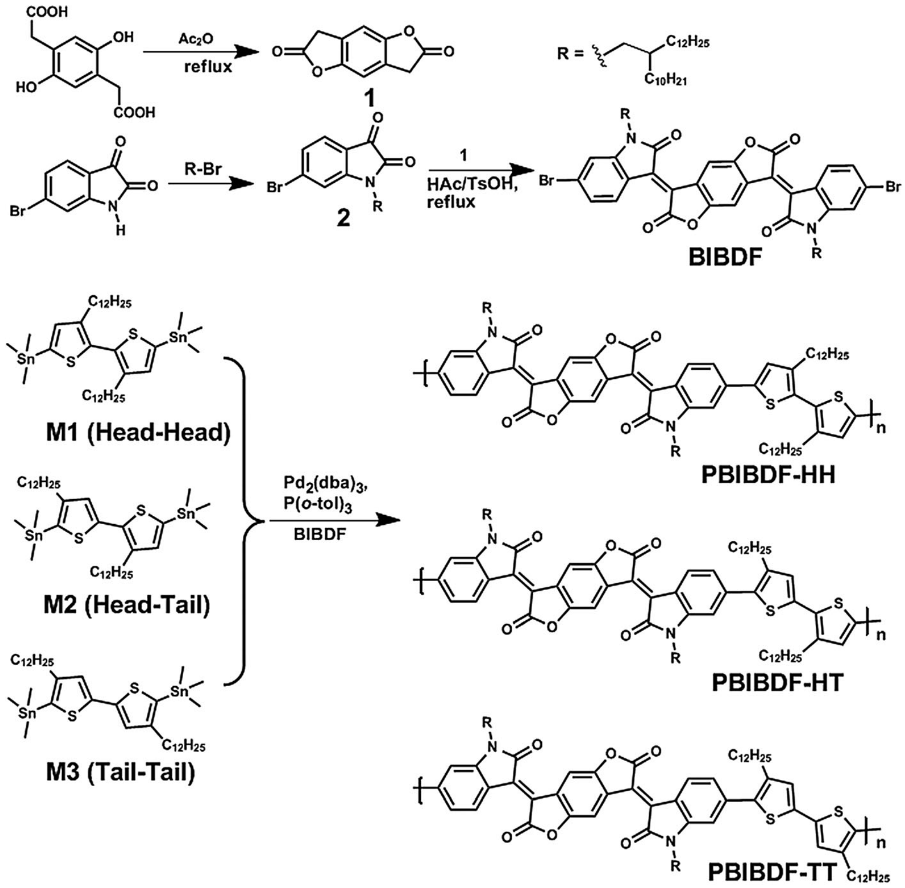

Scheme 1 Synthetic route to the monomer and polymers.

(**PBIBDF-TT**) coupling structures were synthesized *via* the Stille coupling reaction of **BIBDF** with $\mathbf{M_1}$, $\mathbf{M_2}$, and $\mathbf{M_3}$, respectively, at a monomer ratio of 1 : 1 using tris(dibenzylidene-acetone)-dipalladium ($Pd_2(dba)_3$) and tri(*o*-tolyl)phosphine (P(*o*-tolyl)$_3$) as a catalytic system. After cooling to room temperature, the crude polymer was precipitated in methanol and subjected to sequential Soxhlet extraction with methanol and petroleum ether for 24 h each to remove low molecular weight fractions. The residue was then extracted with hot chloroform, distilled under reduced pressure to remove chloroform and dried in vacuum. The GPC plots are shown in Fig. S3–S5 (ESI†) and the corresponding data are listed in Table 1. The number-average molecular weights were 17.4 kDa (PDI = 1.85) for **PBIBDF-HH**, 10.2 kDa (PDI = 1.48) for **PBIBDF-HT**, and 19.4 kDa (PDI = 1.98) for **PBIBDF-TT**. The branched 2-decyltetradecyl chains on the **BIBDF** units and the decyl chains on the bithiophene units were beneficial to the solubility of the final **BIBDF**-based polymer. It is interesting to note that the solubilities of the three polymers differ. Although all three polymers showed good solubility in chlorobenzene and chloroform at room temperature, **PBIBDF-HH** exhibited poor solubility in 1,2,4-trichlorobenzene at room temperature where both **PBIBDF-HT** and **PBIBDF-TT** formed good solutions. Because the three polymers are composed of the same conjugated backbone and have similar molecular weights, their different solubilities indicate that their molecular conformations in solution might be different.

Table 1 Molecular weight of polymers

Polymer	M_n (kDa)	M_w (kDa)	Dispersity
PBIBDF-HH	17.4	32.2	1.85
PBIBDF-HT	10.2	15.2	1.48
PBIBDF-TT	19.4	38.4	1.98

3.2. Optical properties

The molecular conformations of the three **BIBDF**-based polymers were investigated by measuring their absorption spectra both in dilute chloroform solution and in thin films cast from the solution. Fig. 1 displays the normalized UV-vis-NIR absorption spectra of the three polymers. The relevant values of absorption maxima and edges are collected in Table 2. All three polymers exhibit two main absorption bands—both in solution and in thin film—as shown in Fig. 1: band I (300–600 nm) is attributed to the π–π* transitions of the polymer main chains; band II (600–1100 nm) arises from the strong intramolecular charge transfer (ICT) between the electron donating units and the electron withdrawing units.[52] As shown in Fig. 1 and Table 2, there is a significant overlap of band I between all three polymers in solution, but band II diverges significantly. The **PBIBDF-TT** solution shows a blue-shifted ICT peak at 786 nm compared to

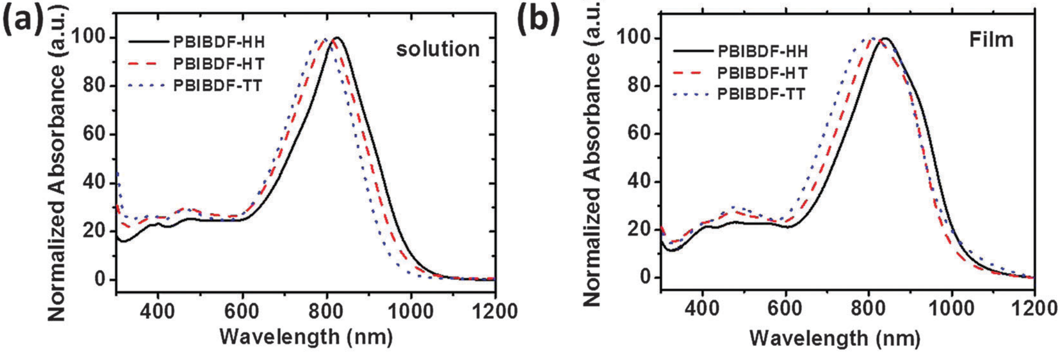

Fig. 1 Normalized UV-vis-NIR absorption spectra of **PBIBDF-HH**, **PBIBDF-HT**, and **PBIBDF-TT** (a) solution in chloroform and (b) thin film.

Table 2 Optical and electrochemical properties of the three BIBDF-based polymers

	$\lambda_{\text{max}}^{\text{abs}}$ (nm)		$\lambda_{\text{onset}}^{\text{abs}}$ (nm)		$E_{\text{g}}^{\text{opt}\,a}$ (eV)				
Polymers	Solution	Film	Solution	Film	Solution	Film	HOMO^{b} (eV)	LUMO^{b} (eV)	$E_{\text{g}}^{\text{ec}\,c}$ (eV)
PBIBDF-HH	825	838	997	1040	1.24	1.19	−5.63	−4.06	1.57
PBIBDF-HT	803	814	970	995	1.28	1.25	−5.68	−4.05	1.63
PBIBDF-TT	786	808	948	998	1.31	1.24	−5.73	−4.01	1.72

[a] $E_{\text{g}}^{\text{opt}} = 1240/\lambda_{\text{onset}}^{\text{abs}}$ (in film). [b] HOMO = $-(4.75 + E_{\text{onset}}^{\text{ox}})$, LUMO = $-(4.75 + E_{\text{onset}}^{\text{red}})$. [c] $E_{\text{g}}^{\text{ec}} = -(\text{HOMO}-\text{LUMO})$.

those of **PBIBDF-HT** (803 nm) and **PBIBDF-HH** (825 nm). Because the conjugated backbones of the three polymers are the same, the blue-shifted absorption implies a shorter conjugated length. The solution absorption spectra indicate that the effective conjugation length and ICT decrease from **PBIBDF-HH** to **PBIBDF-HT** to **PBIBDF-TT**. This change is associated with the position of substituted dodecyl chains, from the sites near the thiophene–thiophene bridge bond to the sites near the **BIBDF**–thiophene bridge bond on the bithiophenes. This effect arises from the backbone torsions (see DFT calculation below) between **BIBDF** and bithiophene units caused by the alkyl chains substituted near the **BIBDF**–thiophene.

As a thin film, the absorption spectrum of **PBIBDF-HH** had a $\lambda_{\text{max}}^{\text{abs}}$ at 838 nm, approximately 13 nm red-shifted compared to the solution-phase peak. From the perspective of steric hindrance, the incorporation of alkyl chains on the 3,3′ sites of bithiophene should produce a large torsion angle, breaking the conjugation and leading to a blue-shift in solution.[49] As the interchain π–π stacking in the solid state suppresses this torsion angle, a red shift over 100 nm was observed between the film and the solution of the isoindigo and bithiophene based polymer. By comparison, a red-shift of ∼13 nm observed for the **PBIBDF-HH** film is small, indicating that **PBIBDF-HH** adopts a similar geometry in both solution and the solid state. The reason may be that the rigid and fused structures of the **BIBDF** and bithiophene monomers reduce the angular torsion in each repeating unit, which is quite different from IID- and DPP-based polymers. **PBIBDF-HT** showed solidification behavior similar to **PBIBDF-HH** with a red-shift of 11 nm between the maximum absorption peak in solution (803 nm) and in the solid state (814 nm). In contrast, the **PBIBDF-TT** film had a $\lambda_{\text{max}}^{\text{abs}}$ at 808 nm and a $\lambda_{\text{onset}}^{\text{abs}}$ at 998 nm. Compared to the solution phase, the absorption spectrum of the **PBIBDF-TT** thin-film exhibited a strong red-shift and an additional absorption shoulder. These observations indicate an improvement in the molecular planarity in the solid phase relative to solution. The optical bandgaps ($E_{\text{g}}^{\text{opt}}$) are calculated from the absorption edges of the solid state films, in other words, a large torsion angle may be present in **PBIBDF-TT**. The $E_{\text{g}}^{\text{opt}}$ of **PBIBDF-HH**, **PBIBDF-HT**, and **PBIBDF-TT** are 1.19, 1.25, and 1.24 eV, respectively.

3.3. Electrochemical properties

The electrochemical properties of the polymers were characterized by cyclic voltammetry (CV). A ferrocene/ferrocenium (Fc/Fc^{+}) redox reaction was used to calibrate the relative potential. Fig. 2 illustrates the CV curves of all three polymers and Table 2 summarizes the corresponding electrochemical data. All these PBIBDFs showed similar LUMO levels around −4.05 eV. But the HOMO levels decreased from −5.63 eV for **PBIBDF-HH** to −5.68 eV for **PBIBDF-HT** and to −5.73 eV for **PBIBDF-TT**. The very low HOMO–LUMO energy levels can be attributed to the electron-deficient lactone and lactam groups on the **BIBDF** unit.

To provide a deeper understanding of the structural and electric parameters of these three polymers, molecular modeling was performed using density functional theory (DFT) calculations. To shorten the calculation time, we projected A–D–A structures to model the π-systems in polymers and the methyl group to model the branched alky side chains. Several local minima structures can be obtained and they are dependent on the starting states. The optimized molecular structures and orbitals of **PBIBDF-HH**, **PBIBDF-HT**, and **PBIBDF-TT** are presented in Fig. 3a. For all three polymers, the **BIBDF** component is composed of large fused aromatic rings and shows a highly planar structure. The differences between the polymers are primarily in the three bridges:

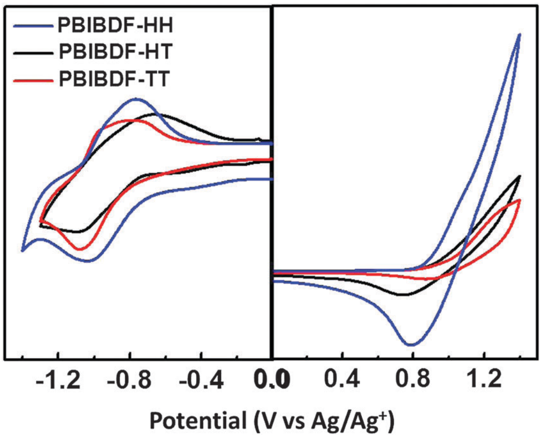

Fig. 2 Cyclic voltammograms of **PBIBDF-HH**, **PBIBDF-HT**, and **PBIBDF-TT** thin films.

two bridges between the **BIBDF** component and thiophene and one bridge between the two thiophenes. Although previous work has demonstrated that the alkyl chains substituted at the 3,3′ sites of bithiophene cause steric hindrance and disrupt the planarity of a conjugated system, we found that the calculated molecular structures of **PBIBDF-HH** are highly dependent on the starting structures. The most stable geometry of **PBIBDF-HH** is quite planar with torsion angles of 0.005–0.3°. Given that the UV-vis-NIR absorption spectra show that **PBIBDF-HH** adopts similar geometries in solution and as a film, the planar geometry is more reasonable than the geometry with a large torsion angle. Otherwise, a large red-shift would be observed between the film and the solution. As the side chain on thiophene moved closer to the **BIBDF** component, the torsion angle between the thiophene and the **BIBDF** component increases dramatically. The two torsion angles between the **BIBDF** component and thiophene are, respectively, 12.9 and 31.0° for **PBIBDF-HT** *versus* 31.8 and 31.8° for **PBIBDF-TT**. These results are consistent with the UV-vis-NIR spectra, indicating that the alkyl chains substituted near the **BIBDF**–thiophene connection cause more steric hindrance than in the case of substitution near the thiophene–thiophene connection. Similar calculation results were obtained by replacing the methyl group on thiophene with a larger butyl group, whose details are given in the ESI,† Fig. S2.

Fig. 3b shows the optimized charge density of the LUMO and the HOMO energy level isosurfaces for **PBIBDF-HH**. The electron clouds of the LUMO level are delocalized along the polymer backbone, while the electron clouds of the HOMO level are primarily localized on the BT units, indicating that charge transfer is preferred. Fig. 3b also illustrates that the HOMO levels of the three polymers decrease in sequence from **PBIBDF-HH** to **PBIBDF-HT** to **PBIBDF-TT**. Their LUMO levels however show no significant shift. Even though DFT calculations provide higher energy-level values than the electrochemical results, both methods present a similar changing tendency.

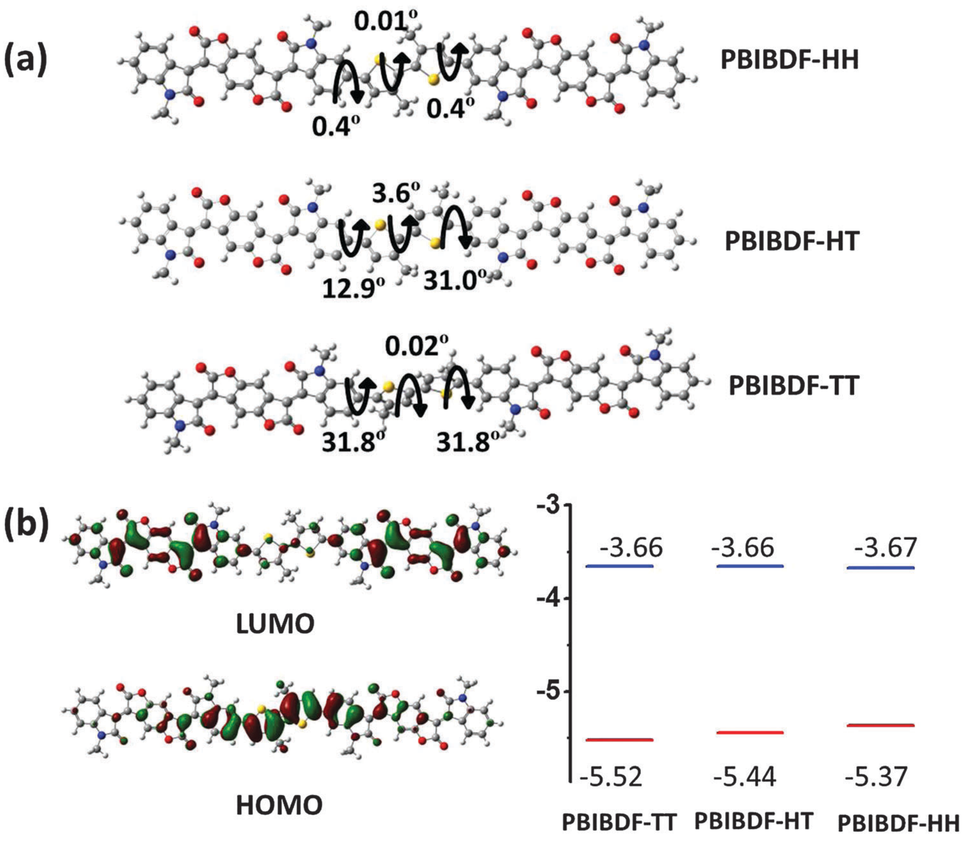

Fig. 3 Density functional theory (DFT) calculations for molecules using Gaussian 09 at the B3LYP/6-31g level.

3.4. OTFT characterization

The charge transport properties of the polymers were investigated by the fabrication of organic thin-film transistors (OTFTs). CYTOP treatment is expected to generate a defect-free surface and obtain the near-intrinsic charge transport properties of three polymers.[53] The representative transfer and output curves of the three PBIBDFs are displayed in Fig. 4. The typical V-shaped transfer curves of all three polymers are indicative of the ambipolar charge transport. The PBIBDF polymers exhibited electron-dominant ambipolar transport due to the highly delocalized LUMO levels and the lower injection barriers for electrons. All polymer FETs exhibited almost hysteresis-free output curves both in electron and hole transport, indicating that traps in all three polymer films are negligible.

Device performances after thermal annealing at different temperatures from 100 °C to 200 °C are summarized in Tables S1 and S2 (ESI†) and Fig. 5. All three PBIBDF polymers showed similar thermal annealing trends, with the device performance improving with increased temperature. This result can be attributed to the improved crystalline ordering and enlarged crystalline domains after annealing. The performances of **PBIBDF-HH** and **PBIBDF-HT** are optimized by thermal annealing at 175 °C, while the performance of **PBIBDF-TT** is optimized at 200 °C. The **PBIBDF-HH** FETs exhibit the best field-effect performance with a maximum electron mobility ($\mu_{e,max}$) of 1.23 cm^2 V^{-1} s^{-1}, an average electron mobility ($\mu_{e,average}$) of 0.86 ± 0.23 cm^2 V^{-1} s^{-1}, a maximum hole mobility ($\mu_{h,max}$) of 0.37 cm^2 V^{-1} s^{-1}, and an average hole mobility ($\mu_{h,average}$) of 0.32 ± 0.04 cm^2 V^{-1} s^{-1}. These values are comparable to the highest mobilities observed for other D–A polymers based on **BIBDF** and its derivatives.[44–48,54–59]

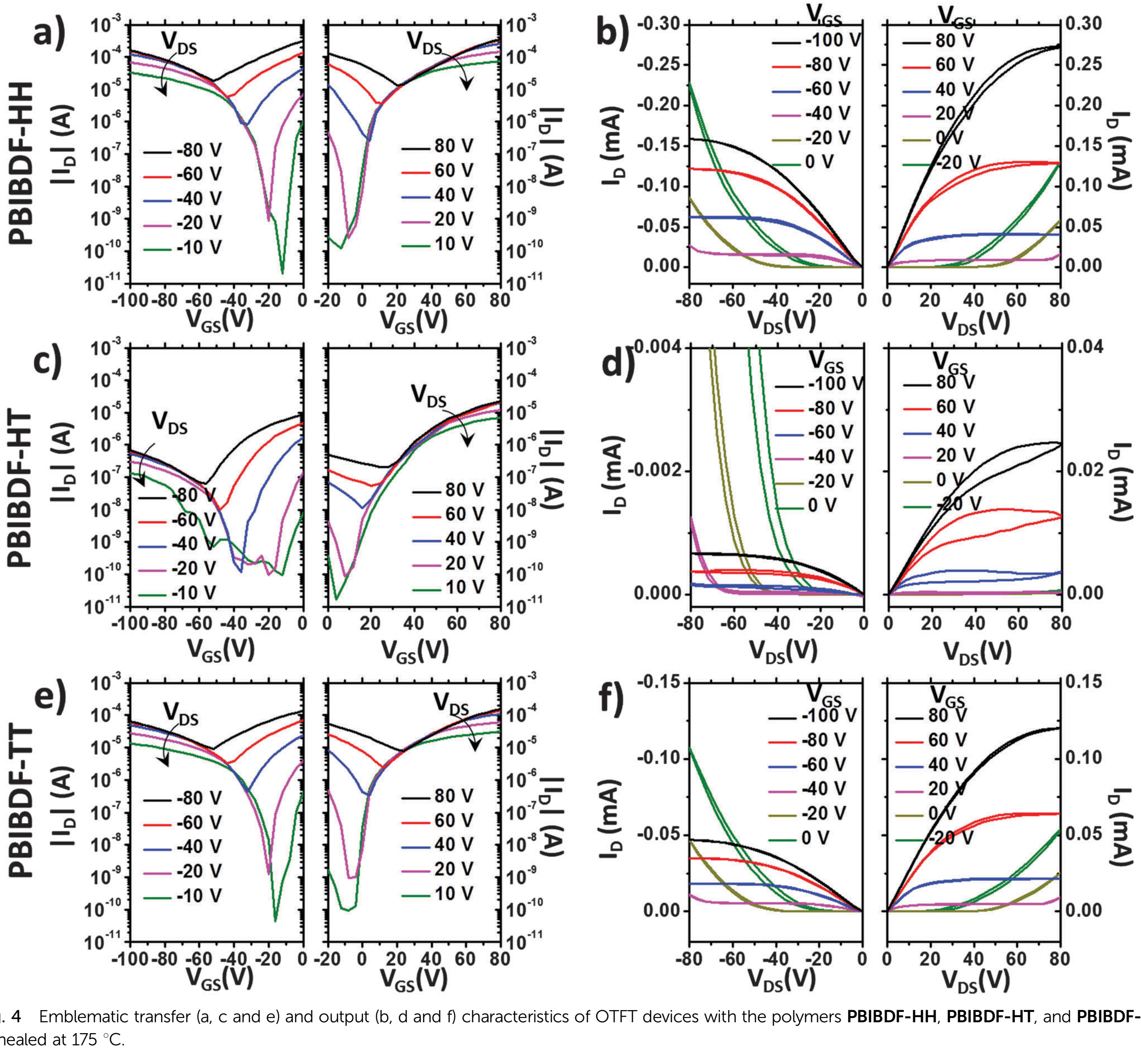

Fig. 4 Emblematic transfer (a, c and e) and output (b, d and f) characteristics of OTFT devices with the polymers **PBIBDF-HH**, **PBIBDF-HT**, and **PBIBDF-TT** annealed at 175 °C.

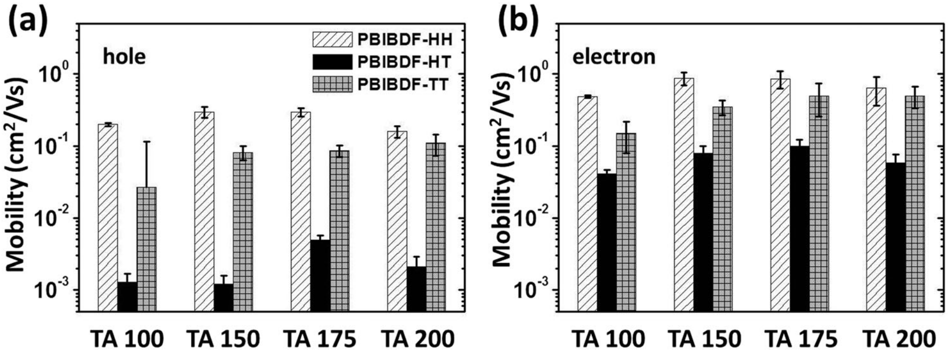

Fig. 5 Mobilities of **PBIBDF-HH**, **PBIBDF-HT**, and **PBIBDF-TT** annealed at 100, 150, 175, and 200 °C.

PBIBDF-TT exhibited a slightly inferior performance with maximum electron and hole mobilities of 0.70 and 0.17 cm^2 V^{-1} s^{-1}, respectively. Unexpectedly, **PBIBDF-HT** films showed a significantly decreased device performance compared with **PBIBDF-HH** and **PBIBDF-TT**. The $\mu_{\text{e,max}}$ and $\mu_{\text{h,max}}$ of **PBIBDF-HT** were only 0.175 and 0.0018 cm^2 V^{-1} s^{-1}, respectively, 10–200 times lower than those of **PBIBDF-HH**.

3.4. Microstructure

The morphologies, crystal structures, and molecular orientations of the semiconductor films critically influence their carrier mobility. The structural features of polymer films were investigated by atomic force microscopy (AFM) (Fig. 6). Nanofibrillar structures were observed in the phase images of all three PBIBDF polymer films, which can act as efficient pathways for charge-carrier transport. A comparison of the films shows that the fibrillar domains of **PBIBDF-HH** were more obvious and more densely packed than those of **PBIBDF-HT** and **PBIBDF-TT**. This difference is closely related to the corresponding differences in field-effect mobility. The **PBIBDF-HT** film, moreover, formed crater-like voids, resulting in the lowest charge transport ability of the three films.

To further investigate the molecular ordering and crystalline characteristics of the film microstructures, two-dimensional grazing-incidence X-ray diffraction (GIXD) was performed (see Fig. 7). The films of **PBIBDF-HH** and **PBIBDF-HT** showed well-defined 5-ordered diffraction peaks of (*h*00) along the q_z (out-of-plane) axis and the (010) diffraction peak along the q_{xy} (in-plane) axis suggesting the formation of a highly ordered edge-on lamellar structure (Fig. 8). In contrast, the out-of-plane and in-plane patterns of **PBIBDF-TT** exhibited both (*h*00) and (010) diffraction peaks, indicating that **PBIBDF-TT** has mixed face-on and edge-on packing. The lamellar spacings were 24.53 Å for **PBIBDF-HH**, 23.61 Å for **PBIBDF-HT**, and 24.72 Å for **PBIBDF-TT**, as calculated from their (100) peaks at q_z = 0.256, 0.266, and 0.254 Å^{-1}. It can be found that the alkyl chain length

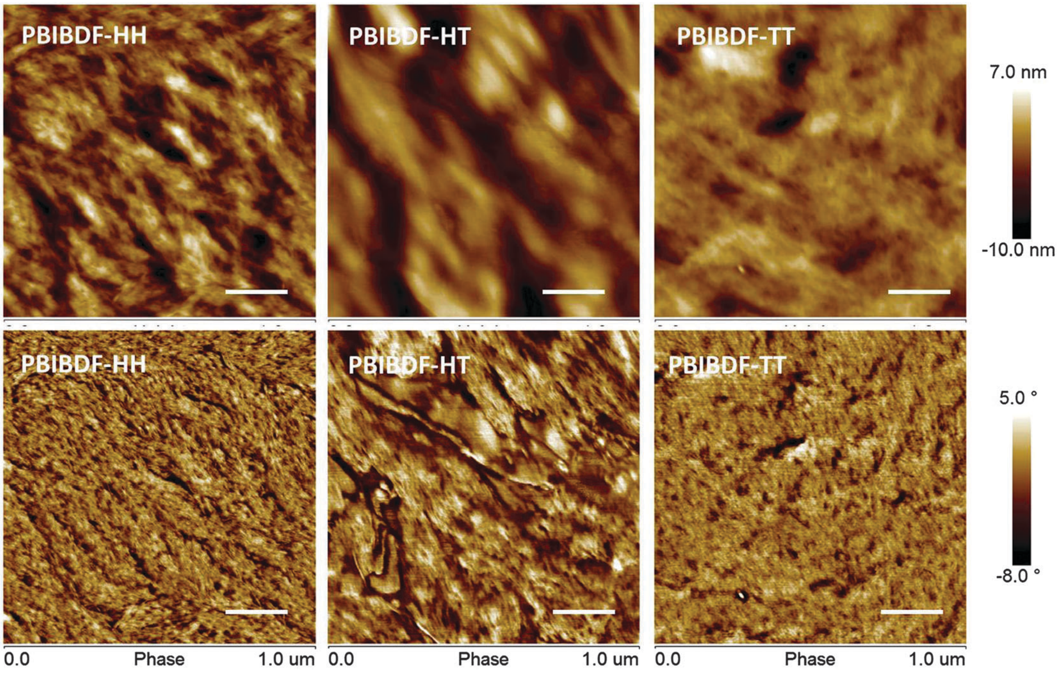

Fig. 6 AFM images of the **PBIBDF-HH**, **PBIBDF-HT**, and **PBIBDF-TT** films annealed at 175 °C.

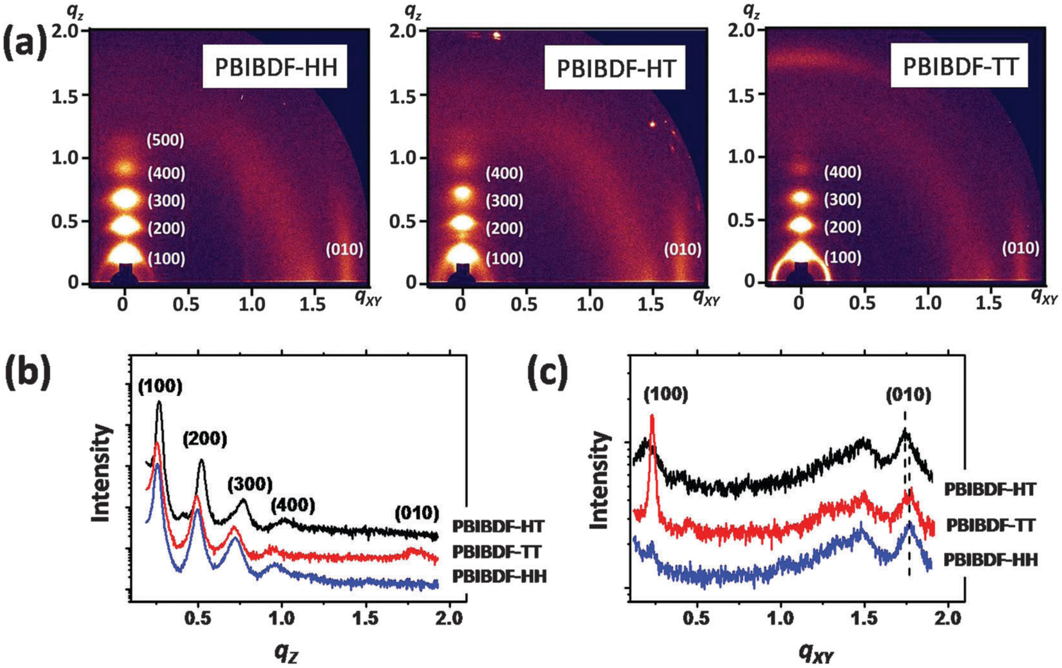

Fig. 7 GIXD patterns of the **PBIBDF-HH**, **PBIBDF-HT**, and **PBIBDF-TT** films annealed at 175 °C.

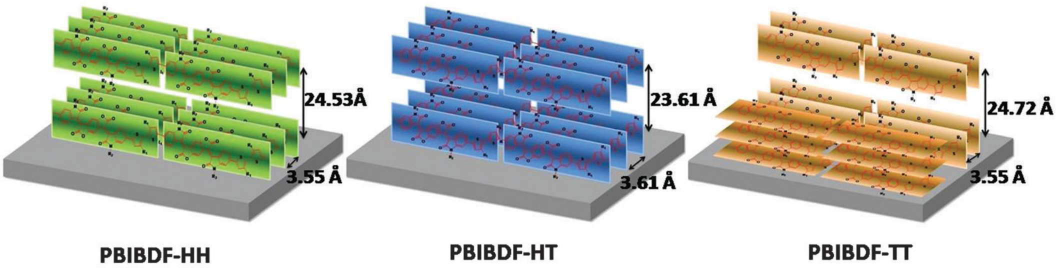

Fig. 8 Recommended polymer packing model in the thin films of three **BIBDF**-based polymers.

in the molecular model is greatly longer than the interlayer distances, indicating that the alkyl chains are folded or tilted in the film state. Among all three **PBIBDF** polymers, **PBIBDF-HT** has the shortest interlayer distance. We ascribe this result to the relatively homogeneous distribution of alkyl chains along the conjugated backbone. The (010) diffraction peaks at q_{xy} = 1.77, 1.77, and 1.74 Å^{-1} for **PBIBDF-HH**, **PBIBDF-TT**, and **PBIBDF-HT**, yield the π–π stacking distances of 3.55 Å, 3.55 Å, and 3.61 Å, respectively. These values are quite small and can only be achieved when the co-planarity of the conjugated backbone is preserved; the high crystallinity and large-scale chain-stacking of films can be contributed to the coefficient of π–π stacking and D–A interaction. It is interesting to note that the π–π stacking distance of 3.61 Å for the **PBIBDF-HT** film is slightly larger than the value of 3.55 Å for the **PBIBDF-HT** and **PBIBDF-TT** films, implying a smaller lamellar spacing. This result is similar to the type I and type II crystal structures of poly(3-alkylthiophene) (P3AT), where the type II crystal structure with fully interdigitated side chains has a larger π–π stacking distance and a smaller lamellar spacing distance than the type I crystal structure with non-interdigitated side chains. Similar to the type II crystal structure of P3AT, the larger π–π stacking distance of the **PBIBDF-HT** film is detrimental to charge transport, resulting in lower field-effect mobility. It should be noted that the relatively lower molecular weight of **PBIBDF-HT** compared with **PBIBDF-HH** and **PBIBDF-TT** may be another unfavorable factor leading to lower mobility.

4. Conclusions

Three **BIBDF** and BT based polymers, **PBIBDF-HH**, **PBIBDF-HT**, and **PBIBDF-TT**, were synthesized to investigate the effect of the side chain position on the microstructure and field-effect properties of **BIBDF**–BT polymers. All three polymers have similar LUMO levels around −4.05 eV, while their HOMO levels exhibit a decreasing trend from −5.63 eV in **PBIBDF-HH** to −5.68 eV in **PBIBDF-HT** to −5.73 eV for **PBIBDF-TT**. DFT calculations suggest that this trend is due to higher steric hindrance from alkyl chains substituted near the **BIBDF**–thiophene connection than those near the thiophene–thiophene connection. A preliminary investigation of OTFT devices with the three polymers was also performed. **PBIBDF-HH**-based devices produced the highest electron mobility, 1.23 $cm^2 V^{-1} s^{-1}$, and the highest hole mobility, 0.37 $cm^2 V^{-1} s^{-1}$. Polymer-packing structures investigated using GIXD and AFM were correlated with the substitution position dependent carrier mobility of the three polymers. **PBIBDF-HH** and **PBIBDF-HT** adopted edge-on packing models and **PBIBDF-TT** displayed a mixture of face-on and edge-on packing. The π–π stacking distance of 3.61 Å for the **PBIBDF-HT** film however is slightly larger than the value of 3.55 Å for the **PBIBDF-HT** and **PBIBDF-TT** films, implying a smaller lamellar spacing detrimental to charge transport, resulting in a lower field-effect mobility.

Acknowledgements

This work was supported by National Natural Science Foundation of China (NSFC Grant No. 51573036 and 21174036) and Program for New Century Excellent Talents in University (Grant No. NCET-12-0839). The authors thank 3C beamlines (the Pohang Accelerator Laboratory in Korea) and BL16B beamlines (the Shanghai Synchrotron Radiation Facility in China) for providing the beam time.

References

1 H. Yan, Z. Chen, Y. Zheng, C. Newman, J. R. Quinn, F. Dotz, M. Kastler and A. Facchetti, *Nature*, 2009, **457**, 679–686.

2 C. Wang, H. Dong, W. Hu, Y. Liu and D. Zhu, *Chem. Rev.*, 2012, **112**, 2208–2267.

3 A. C. Arias, J. D. MacKenzie, I. McCulloch, J. Rivnay and A. Salleo, *Chem. Rev.*, 2010, **110**, 3–24.

4 Q. Meng and W. Hu, *Phys. Chem. Chem. Phys.*, 2012, **14**, 14152–14164.

5 X. Gao and Z. Zhao, *Sci. China: Chem.*, 2015, **58**, 947–968.

6 S. Holliday, J. E. Donaghey and I. McCulloch, *Chem. Mater.*, 2014, **26**, 647–663.

7 H.-R. Tseng, H. Phan, C. Luo, M. Wang, L. A. Perez, S. N. Patel, L. Ying, E. J. Kramer, T.-Q. Nguyen, G. C. Bazan and A. J. Heeger, *Adv. Mater.*, 2014, **29**, 2993–2998.

8 G. Kim, S.-J. Kang, G. K. Dutta, Y.-K. Han, T. J. Shin, Y.-Y. Noh and C. Yang, *J. Am. Chem. Soc.*, 2014, **136**, 9477–9483.

9 J. Li, Y. Zhao, H. S. Tan, Y. Guo, C.-A. Di, G. Yu, Y. Liu, M. Lin, S. H. Lim, Y. Zhou, H. Su and B. S. Ong, *Sci. Rep.*, 2012, **2**, 754.

10 I. Kang, H.-J. Yun, D. S. Chung, S.-K. Kwon and Y.-H. Kim, *J. Am. Chem. Soc.*, 2013, **135**, 14896–14899.

11 D. Venkateshvaran, M. Nikolka, A. Sadhanala, V. Lemaur, M. Zelazny, M. Kepa, M. Hurhangee, A. J. Kronemeijer, V. Pecunia, I. Nasrallah, I. Romanov, K. Broch, I. McCulloch, D. Emin, Y. Olivier, J. Cornil, D. Beljonne and H. Sirringhaus, *Nature*, 2014, **515**, 384–388.

12 A. J. Kronemeijer, E. Gili, M. Shahid, J. Rivnay, A. Salleo, M. Heeney and H. Sirringhaus, *Adv. Mater.*, 2012, **24**, 1558–1565.

13 Z. Fei, P. Pattanasattayavong, Y. Han, B. C. Schroeder, F. Yan, R. J. Kline, T. D. Anthopoulos and M. Heeney, *J. Am. Chem. Soc.*, 2014, **136**, 15154–15157.

14 H.-J. Yun, S.-J. Kang, Y. Xu, S. O. Kim, Y.-H. Kim, Y.-Y. Noh and S.-K. Kwon, *Adv. Mater.*, 2014, **26**, 7300–7307.

15 H. N. Tsao, D. M. Cho, I. Park, M. R. Hansen, A. Mavrinskiy, D. Y. Yoon, R. Graf, W. Pisula, H. W. Spiess and K. Mullen, *J. Am. Chem. Soc.*, 2011, **133**, 2605–2612.

16 X. Guo, F. S. Kim, M. J. Seger, S. A. Jenekhe and M. D. Watson, *Chem. Mater.*, 2012, **24**, 1434–1442.

17 N. B. Kolhe, A. Z. Ashar, K. S. Narayan and S. K. Asha, *Macromolecules*, 2014, **47**, 2296–2305.

18 A. Luzio, D. Fazzi, F. Nuebling, R. Matsidik, A. Straub, H. Komber, E. Giussani, S. E. Watkins, M. Barbatti, W. Thiel, E. Gann, L. Thomsen, C. R. McNeill, M. Caironi and M. Sommer, *Chem. Mater.*, 2014, **26**, 6233–6240.

19 V. Senkovskyy, R. Tkachov, H. Komber, M. Sommer, M. Heuken, B. Voit, W. T. S. Huck, V. Kataev, A. Petr and A. Kiriy, *J. Am. Chem. Soc.*, 2011, **133**, 19966–19970.

20 M. M. Szumilo, E. H. Gann, C. R. McNeill, V. Lemaur, Y. Oliver, L. Thomsen, Y. Vaynzof, M. Sommer and H. Sirringhaus, *Chem. Mater.*, 2014, **26**, 6796–6804.

21 B. Kang, R. Kim, S. B. Lee, S.-K. Kwon, Y.-H. Kim and K. Cho, *J. Am. Chem. Soc.*, 2016, **138**, 3679–3686.

22 J. Fan, J. D. Yuen, M. Wang, J. Seifter, J.-H. Seo, A. R. Mohebbi, D. Zakhidov, A. Heeger and F. Wudl, *Adv. Mater.*, 2012, **24**, 2186–2190.

23 J. D. Yuen, J. Fan, J. Seifter, B. Lim, R. Hufschmid, A. J. Heeger and F. Wudl, *J. Am. Chem. Soc.*, 2011, **133**, 20799–20807.

24 H. Bronstein, Z. Chen, R. S. Ashraf, W. Zhang, J. Du, J. R. Durrant, P. S. Tuladhar, K. Song, S. E. Watkins, Y. Geerts, M. M. Wienk, R. A. J. Janssen, T. Anthopoulos, H. Sirringhaus, M. Heeney and I. McCulloch, *J. Am. Chem. Soc.*, 2011, **133**, 3272–3275.

25 X. Guo, S. R. Puniredd, B. He, T. Marszalek, M. Baumgarten, W. Pisula and K. Muellen, *Chem. Mater.*, 2014, **26**, 3595–3598.

26 J. S. Ha, K. H. Kim and D. H. Choi, *J. Am. Chem. Soc.*, 2011, **133**, 10364–10367.

27 J. W. Jung, F. Liu, T. P. Russell and W. H. Jo, *Energy Environ. Sci.*, 2012, **5**, 6857–6861.

28 C. Kanimozhi, N. Yaacobi-Gross, K. W. Chou, A. Amassian, T. D. Anthopoulos and S. Patil, *J. Am. Chem. Soc.*, 2012, **134**, 16532–16535.

29 K.-H. Kim, S. Park, H. Yu, H. Kang, I. Song, J. H. Oh and B. J. Kim, *Chem. Mater.*, 2014, **26**, 6963–6970.

30 J. S. Lee, S. K. Son, S. Song, H. Kim, D. R. Lee, K. Kim, M. J. Ko, D. H. Choi, B. Kim and J. H. Cho, *Chem. Mater.*, 2012, **24**, 1316–1323.

31 Y. Li, S. P. Singh and P. Sonar, *Adv. Mater.*, 2010, **22**, 4862–4866.

32 T. L. Nelson, T. M. Young, J. Liu, S. P. Mishra, J. A. Belot, C. L. Balliet, A. E. Javier, T. Kowalewski and R. D. McCullough, *Adv. Mater.*, 2010, **22**, 4617–4621.

33 P. Sonar, T. R. B. Foong, S. P. Singh, Y. Li and A. Dodabalapur, *Chem. Commun.*, 2012, **48**, 8383–8385.

34 X. Zhang, L. J. Richter, D. M. DeLongchamp, R. J. Kline, M. R. Hammond, I. McCulloch, M. Heeney, R. S. Ashraf, J. N. Smith, T. D. Anthopoulos, B. Schroeder, Y. H. Geerts, D. A. Fischer and M. F. Toney, *J. Am. Chem. Soc.*, 2011, **133**, 15073–15084.

35 T. Lei, Y. Cao, Y. L. Fan, C. J. Liu, S. C. Yuan and J. Pei, *J. Am. Chem. Soc.*, 2011, **133**, 6099–6101.

36 J. Mei, D. H. Kim, A. L. Ayzner, M. F. Toney and Z. Bao, *J. Am. Chem. Soc.*, 2011, **133**, 20130–20133.

37 R. S. Ashraf, A. J. Kronemeijer, D. I. James, H. Sirringhaus and I. McCulloch, *Chem. Commun.*, 2012, **48**, 3939–3941.

38 B. He, A. B. Pun, D. Zherebetskyy, Y. Liu, F. Liu, L. M. Klivansky, A. M. McGough, B. A. Zhang, K. Lo, T. P. Russell, L. Wang and Y. Liu, *J. Am. Chem. Soc.*, 2014, **136**, 15093–15101.

39 S. Himmelberger, D. T. Duong, J. E. Northrup, J. Rivnay, F. P. V. Koch, B. S. Beckingham, N. Stingelin, R. A. Segalman, S. C. B. Mannsfeld and A. Salleo, *Adv. Funct. Mater.*, 2015, **25**, 2616–2624.

40 C.-Y. Kuo, Y.-C. Huang, C.-Y. Hsiow, Y.-W. Yang, C.-I. Huang, S.-P. Rwei, H.-L. Wang and L. Wang, *Macromolecules*, 2013, **46**, 5985–5997.

41 J. Mei, H.-C. Wu, Y. Diao, A. Appleton, H. Wang, Y. Zhou, W.-Y. Lee, T. Kurosawa, W.-C. Chen and Z. Bao, *Adv. Funct. Mater.*, 2015, **25**, 3455–3462.

42 J. Y. Back, T. K. An, Y. R. Cheon, H. Cha, J. Jang, Y. Kim, Y. Baek, D. S. Chung, S.-K. Kwon, C. E. Park and Y.-H. Kim, *ACS Appl. Mater. Interfaces*, 2015, **7**, 351–358.

43 J. Mei and Z. Bao, *Chem. Mater.*, 2014, **26**, 604–615.

44 T. Lei, J.-H. Dou, X.-Y. Cao, J.-Y. Wang and J. Pei, *J. Am. Chem. Soc.*, 2013, **135**, 12168–12171.

45 G. B. Zhang, J. H. Guo, M. Zhu, P. Li, H. B. Lu, K. Cho and L. Z. Qiu, *Polym. Chem.*, 2015, **6**, 2531–2540.

46 Z. Yan, B. Sun and Y. Li, *Chem. Commun.*, 2013, **49**, 3790–3792.

47 T. Lei, J.-H. Dou, X.-Y. Cao, J.-Y. Wang and J. Pei, *Adv. Mater.*, 2013, **25**, 6589–6593.

48 G. B. Zhang, P. Li, L. X. Tang, J. X. Ma, X. H. Wang, H. B. Lu, B. Kang, K. Cho and L. Z. Qiu, *Chem. Commun.*, 2014, **50**, 3180–3183.

49 T. Lei, Y. Cao, X. Zhou, Y. Peng, J. Bian and J. Pei, *Chem. Mater.*, 2012, **24**, 1762–1770.

50 E. Bundgaard and F. C. Krebs, *Polym. Bull.*, 2005, **55**, 157–164.

51 I. Osaka, G. Sauve, R. Zhang, T. Kowalewski and R. D. McCullough, *Adv. Mater.*, 2007, **19**, 4160–4165.

52 X. Guo, A. Facchetti and T. J. Marks, *Chem. Rev.*, 2014, **114**, 8943–9021.

53 H.-J. Yun, H. H. Choi, S.-K. Kwon, Y.-H. Kim and K. Cho, *Chem. Mater.*, 2014, **26**, 3928–3937.

54 Y. Jiang, Y. Gao, H. Tian, J. Ding, D. Yan, Y. Geng and F. Wang, *Macromolecules*, 2016, **49**, 2135–2144.

55 X. Zhou, N. Ai, Z.-H. Guo, F.-D. Zhuang, Y.-S. Jiang, J.-Y. Wang and J. Pei, *Chem. Mater.*, 2015, **27**, 1815–1820.

56 G. Zhang, Z. Ye, P. Li, J. Guo, Q. Wang, L. Tang, H. Lu and L. Qiu, *Polym. Chem.*, 2015, **6**, 3970–3978.

57 Y. He, C. Guo, B. Sun, J. Quinn and Y. Li, *Chem. Commun.*, 2015, **51**, 8093–8096.

58 Y. Deng, B. Sun, Y. He, J. Quinn, C. Guo and Y. Li, *Chem. Commun.*, 2015, **51**, 13515–13518.

59 Y. Cao, J.-S. Yuan, X. Zhou, X.-Y. Wang, F.-D. Zhuang, J.-Y. Wang and J. Pei, *Chem. Commun.*, 2015, **51**, 10514–10516.